Synthetic Metals 161 (2011) 431–439

Contents lists available at ScienceDirect

Synthetic Metals

journal homepage: www.elsevier.com/locate/synmet

Picosecond laser patterning of PEDOT:PSS thin films

N.G. Semaltianos[a,*], C. Koidis[a], C. Pitsalidis[a], P. Karagiannidis[a], S. Logothetidis[a], W. Perrie[b], D. Liu[b], S.P. Edwardson[b], E. Fearon[b], R.J. Potter[b], G. Dearden[b], K.G. Watkins[b]

[a] Department of Physics, Aristotle University of Thessaloniki, Thessaloniki, GR-54124, Greece
[b] Department of Engineering, University of Liverpool, Brownlow Hill, Liverpool L69 3GH, UK

ARTICLE INFO

Article history:
Received 31 July 2010
Received in revised form
26 November 2010
Accepted 16 December 2010
Available online 15 January 2011

Keywords:
PEDOT:PSS
Laser patterning
Raman spectroscopy
Spectroscopic Ellipsometry

ABSTRACT

Picosecond pulsed laser (10.4 ps, 1064 nm, 5 and 50 kHz) patterning studies were performed, of PEDOT:PSS thin films of varying thickness deposited by spin coating on glass substrates, by ablating the films or by changing locally by laser irradiation the optical and electrical properties of the polymer. From a detailed observation of the morphology of single pulse ablated holes on the surfaces of the films, in combination with simple calculations, it is concluded that photomechanical ablation is the likely ablation mechanism of the films. The single pulse ablation thresholds were measured equal to 0.13–0.18 J/cm^2 for films with thicknesses in the region of ~100–600 nm. The implications on ablation line patterning of the films using different fluences, scanning speeds and pulse repetition rates, were investigated systematically. Laser irradiation of the films before ablation induces a metal–insulator transition of the polymer because of the formation of charge localization due to a possible creation of molecular disorder in the polymer and shortening of its conjugation length.

1. Introduction

PEDOT:PSS [poly(3,4-ethylenedioxythiophene):poly(4-styrenesulfonate)] is a conductive polymer blend which finds applications as an antistatic coating of photographic films and recording tapes, dust protective coating of plastic parts, clean room packaging material, as a housing and window material of plastic electronic components and as a glass coating of the monitors and TV screens [1]. This is because, it combines a relatively high electrical conductivity with transparency in the visible spectral range, low cost, flexibility and good adhesion. Highly conductive formulations of the polymer are also used in electrochromic windows, as transparent conductors in inorganic electroluminescent devices (zinc sulphide/barium titanate) and as anode electrodes (hole injection/transport layer) in flexible organic electronic devices such as light emitting diodes, field effect transistors and photovoltaic cells usually as a replacement of the traditionally used indium tin oxide (ITO) or on top of it to smooth its surface and improve device stability [2].

In these applications, patterning of the polymer film is often required. Traditional methods for patterning PEDOT:PSS films, include photoexposure of prepolymers followed by a wet chemical developing step, wet photochemical or photo-electrochemical polymerization [3], selective overoxidation [4], the so-called "line patterning" [5] as well as oxygen plasma etching through a metallic contact mask [6]. These methods usually involve chemically intensive multiple etching steps, post-fabrication cleaning procedures and the use of prefabricated masks which increase the cost, labour, processing time and toxic wastes.

An alternative advantageous technology for direct patterning including texturing by ablation and machining as well as changing in a controlled way the properties of polymeric materials in general, in bulk or a thin film form, involves the utilization of intense laser sources. Among them, the ultrashort pulse lasers (with pulse widths in the femtosecond regime) which in the ablation and machining of metals offer the advantages of the absence or minimization of a thermal and collateral damage (reduced heat-affected zone) as well as lower ablation thresholds as compared to long pulse nanosecond lasers, play a dominant role also in the ablative patterning of polymers. For instance, thermal damage free ablation of polytetrafluoroethylene (PTFE (Teflon)) has been reported using 170 fs pulses at 798 nm from a Ti:Sapphire laser [7] or 300 fs at 248 nm from an excimer laser [8] while the polymer surface was found to be severely degraded and disrupted when using 16 ns pulses at 248 nm [8]. High quality ablated area was obtained on polyethylene terephthalate (PET) and polyimide (PI) films using 500 fs pulses at 248 nm from a KrF laser [9] or 150 fs pulses at 800 nm from a Ti:Sapphire laser [10]. Dye doped poly(methyl methacrylate) (PMMA) films of a few micrometers thick on glass substrates were ablated using 150 ps duration pulses from a 1064 nm YAG laser [11]. The film thickness ablation rate and change of the optical transmission of a variety of organic thin films

* Corresponding author.
E-mail address: semal@physics.auth.gr (N.G. Semaltianos).

0379-6779/$ – see front matter © 2010 Elsevier B.V. All rights reserved.
doi:10.1016/j.synthmet.2010.12.022

such as diacetylenes, polystyrene and polycarbonate, which are of interest in the fabrication of optoelectronic devices and as resists, were investigated by UV–visible (193, 248 or 532 nm), picosecond (50 ps) and nanosecond (20 ns) laser photoablation [12]. Fine channels as narrow as 2.2–6 μm were ablation patterned on PEDOT:PSS thin films (thicknesses = 62–1900 nm) on Au/Pd substrates using a 1.5 cm focal length lens to focus 150 fs pulses at 775 nm from a Ti:Sapphire laser [13].

Although using femtosecond laser sources for micromachining applications seems as a directly advantageous technology, however these laser systems are quite expensive, complex and massive systems. They also suffer from low efficiencies because direct diode pumping is not possible. Thus in the last few years there is a general trend in trying to optimize the use of laser sources with *picosecond* pulse duration instead, for materials micromachining applications, due to the fact that these sources are inexpensive, simple, reliable and stable compact systems and thus better suited for industrial applications and also because there are expectations that these lasers will offer machining quality comparable to the one achieved with femtosecond lasers. A few characteristic examples of previous works where laser sources were used to pattern polymeric materials by locally changing their electrical or optical properties include irradiation using 30 ns, 0.5–8 Hz pulses at 248 nm from a KrF laser, of originally insulating PI films, which induced an increase of the electrical conductivity of the polymer by a few orders of magnitude [14], or irradiation using a 488 nm CW-argon ion or 351 nm XeF laser of originally insulating poly(bis-alkylthio-acetylene) (PATAC) films [15]. Irradiation of PMMA using an excimer laser at 193, 248 or 308 nm caused an increase of the refractive index of the polymer [16].

This paper involves laser patterning of PEDOT:PSS thin films by ablation (removal) or a by a local change of the optical and electrical properties of the polymer, using a picosecond laser source (pulse width = 10.4 ps, laser wavelength = 1064 nm, pulse repetition rates = 5 and 50 kHz). From observations of the surface morphology of single pulse ablated holes (and of their surrounding areas) in combination with simple calculations of the relevant time constants involved in the energy absorption and propagation in relation to the width of the laser pulse, the picosecond laser ablation mechanism of the PEDOT:PSS thin films is elucidated and discussed. The dependence on film thickness of the single pulse picosecond laser ablation threshold of the film has been established. Line ablation patterning of the thin films is investigated using different laser fluences, scanning parameters and pulse repetition rates. Finally, the electrical conductivities of laser irradiated films before ablation, have been measured and correlated to the surface morphology and polymer Raman and Ellipsometric spectroscopic characteristics.

2. Experimental details

A High-Q picosecond laser was used in this work. This consists of a solid state diode pumped Nd:Vanadate (Nd:YVO_4) oscillator at 1064 nm and a high power regenerative amplifier (IC381) followed by a pulse picker. The laser is controlled via a computer interface (HQL GUI software). This system can produce pulses at the main wavelength of 1064 nm with 10.4 ps pulse FWHM and maximum average powers of 1200 and 2400 mW (stability = 0.7% RMS (15 h)) at chosen pulse repetition rates of 5 and 50 kHz, respectively. Beam intensity spatial profile is Gaussian (TEM_{00} mode) with $M_x^2 = 1.12$ and $M_y^2 = 1.14$. More details of the laser system are given in Ref.

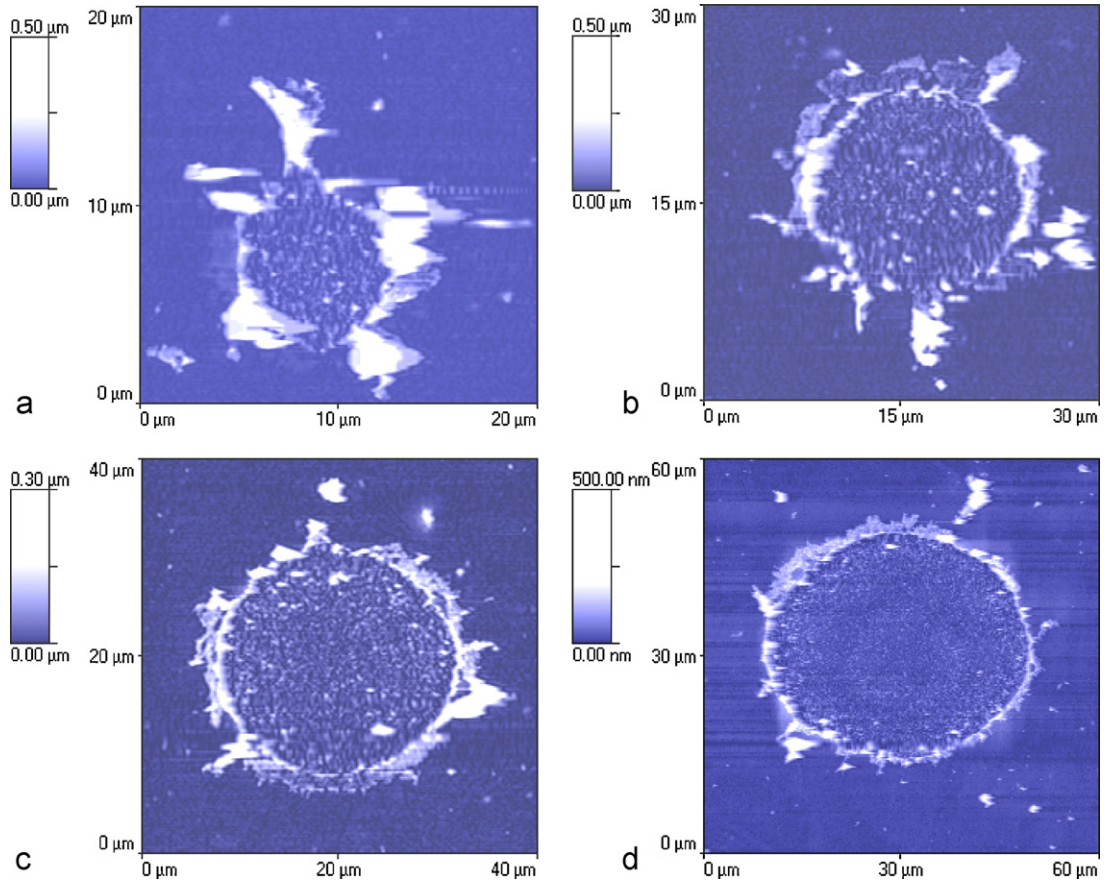

Fig. 1. Typical AFM topography images of single pulse ablated holes on the films (film spin coated at 2000 rpm) with fluences of: 0.23 J/cm^2 (a), 0.35 J/cm^2 (b), 0.74 J/cm^2 (c) and 2.64 J/cm^2 (d), respectively.

[17]. The beam was focused onto the film surface using a telecentric f–θ lens (f = 100 mm) AR coated for the IR, passing previously through a Scanning Galvo head (SGLV) (GSI Lumonics). Scan patterns were software generated using the software SCAPS GmbH and the SCANLAB RTC® 4 PC interface board. The flat field region is approximately 70 mm × 70 mm. The spot size $2w_0$ ($1/e^2$) diameter at the focal plane was estimated to be ~28 μm from observed single pulse ablated holes (straight line fitting in a plot of D^2 versus $\ln(E_p)$).

The formulation of PEDOT:PSS, CLEVIOS™ FE which was bought from H.C. Starck [18] was used in this work. As is the case for oxidized highly conductive forms of PEDOT:PSS, this formulation exhibits a steadily increasing absorption above 800 nm due to the low energy charge carriers (radical cations and dications) [19,18]. The polymer was deposited on glass substrates which were pre-cleaned by ultrasonication for 10 min each time in acetone, isopropanol and methanol followed by UV-irradiation for another 10 min, by spin coating at 400 rpm for 6 s in order to first spread the polymer on the substrate surface and subsequently at 500, 600, 800, 1000, 2000 and 4000 rpm for 30 s for each film and finally dried out on a hot plate at 90 °C for 10 min. The corresponding thicknesses of the films, determined by Spectroscopic Ellipsometry (SE) measurements in Vis–farUV using a Jobin-Yvon instrument, were: 564 ± 34, 465 ± 18, 422 ± 7, 280 ± 13, 128 ± 5 and 95 ± 4 nm, respectively. The samples were positioned onto an Aerotech moving stage which could be moved in the x, y and z directions with accuracy of ±0.5 nm (however in this work patterning of the films was done by moving only the beam with the SGLV onto the surface of a stationary sample). For a detailed 3D high resolution characterization of single pulse ablated holes on the films, Atomic Force Microscopy (AFM) imaging and measurements were performed in non-contact mode using Si cantilevers with radius of curvature less than 10 nm. Laser fabricated ablation lines on the film surfaces were imaged by white light scanning interferometric microscopy using a Wyko NT1100 instrument. Raman spectra of the films were acquired using a Jobin Yvon HR800 system (pumping beam at λ = 514.48 nm) with a CCD detector. The resistances of the films were measured using the Van der Pauw method at four point contact configuration using a Keithley 2400 source/meter [20].

3. Results and discussion

3.1. Single pulse ablation thresholds

The single pulse picosecond laser ablation thresholds of the films which represent the minimum laser fluence required to initiate ablation with the first laser pulse were determined, by ablating a series of holes on the film surfaces with different pulse energies. To obtain holes corresponding to single pulses, the beam was scanned along a line pattern but with a speed ≥300 mm/s. In this way by taking into account the pulse length (10.4 ps) and pulse repetition rate of 5 kHz, a series of holes with centre to centre distances between them of ~60 μm along the line length was obtained which were isolated from each other considering that the beam diameter at the focal point of the f–θ lens is ~28 μm.

Typical AFM images of a series of single pulse ablated holes on the films for different fluences are shown in Fig. 1. The images in Fig. 1 were taken in non-contact mode and thus they represent the topography of the ablated holes and their surrounding areas which is formed directly by the ablation. It is seen that the material which is removed from the hole by the ablation and accumulated around its perimeter does not remind melted and resolidified material and there is no phase-change redeposited debris around the ablated holes. The ablated material has rather the form of lifted-off "flakes" which are still attached onto the original film. This indicates that the ablation is mainly via some kind of mechanical fracture and subsequent explosive ejection (spallation) of the film from the substrate surface rather than vaporization or melting and resolidification or other phase change induced ablation. The polymer film is ablated by photomechanical ablation (or stress-assisted ablation) [21]. This kind of ablation takes place when both

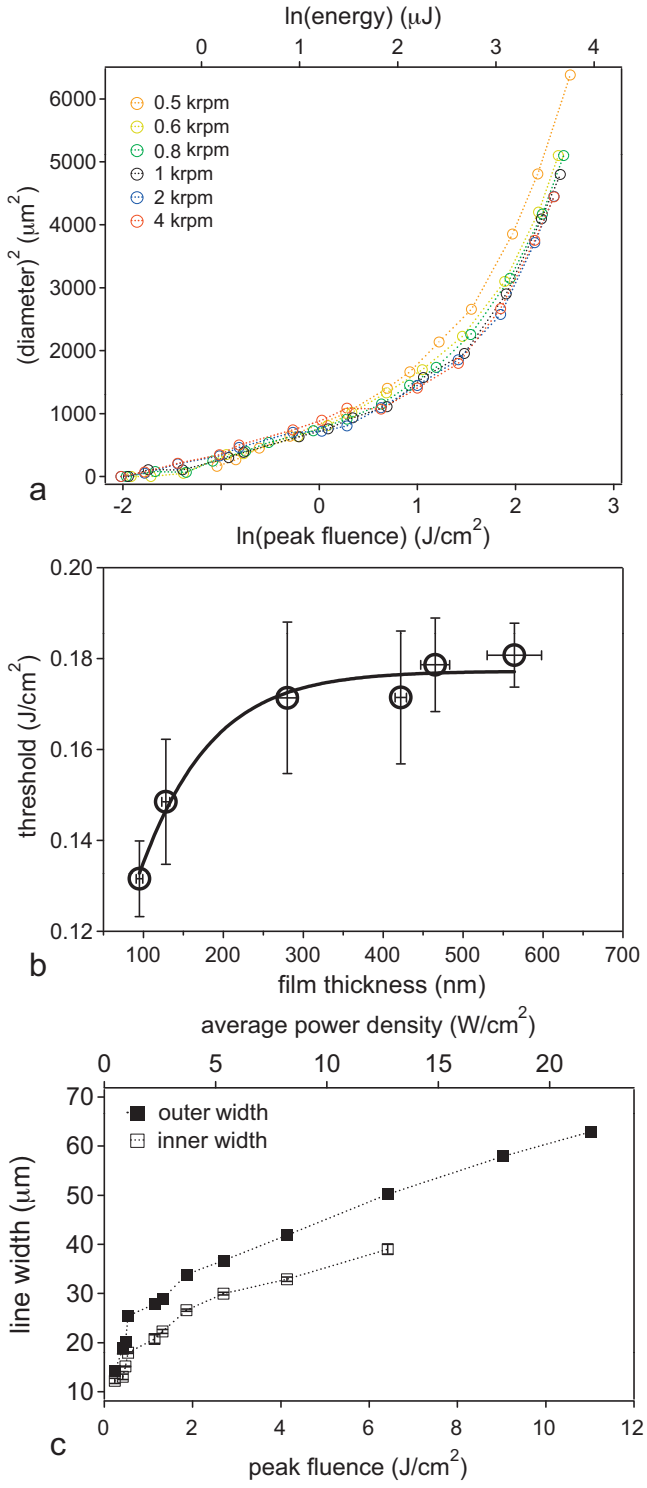

Fig. 2. (a) Plot of the square of the diameter of single pulse ablated holes versus logarithm of peak fluence (bottom scale) and logarithm of pulse energy (top scale) for the films with different thicknesses, (b) single pulse ablation threshold versus film thickness, and (c) inner and outer patterned line width versus peak fluence (bottom scale) and average power density (top scale) (f = 5 kHz, υ = 30 mm/s).

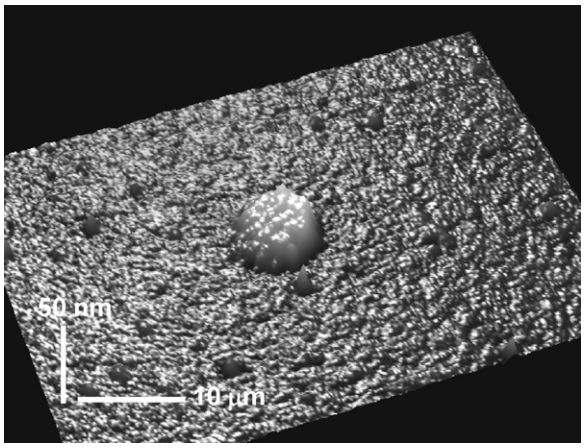

Fig. 3. Typical image of a laser formed blister on the films surfaces (film spin coated at 2000 rpm, $F = 0.15\,J/cm^2$).

the laser energy is absorbed strongly in a very localized area on the film, without any considerable thermal conduction losses away from the irradiated area (thermal confinement) and the heating is so rapid as to produce a transient thermoelastic stress larger than the film fracture limit, i.e. before any thermal expansion allows for stress relaxation (stress or inertial confinement). The resulting transient and quasi-static thermoelastic stresses can cause weakening, fracture and ejection of the material. Quantitatively, if the laser temporal pulse width τ is shorter than both the thermal relaxation time: $\tau_{th} = d^2/4\chi$ and the acoustic relaxation time: $\tau_{ac} = d/c_s$, then both of the above confinement criteria are satisfied [21]. In the above relations d is the smallest dimension of the heated volume (either the beam diameter or the optical penetration depth, whichever is smaller), χ is the thermal diffusivity of the film material and c_s the speed of sound in the film. By considering at the present case of PEDOT:PSS films the set of parameters: thermal conductivity $\kappa = 0.17\,W\,m^{-1}\,K^{-1}$ [22], density $\rho \approx 1\,g/ml$, specific heat capacity $C_P = 9.94\,J\,kg^{-1}\,K^{-1}$ [23], the thermal diffusivity of the films is determined as: $\chi \equiv \kappa/\rho C_P = 17.12 \times 10^{-6}\,m^2\,s^{-1}$. Since the beam diameter is always greater than the film thickness (even for the thicker film), the thermal relaxation time is estimated equal to: $\tau_{th} \approx 146\,ps$ (for a film with an average thickness ~100 nm). Furthermore, considering a shear stress = 25 MPa and a shear strain = 0.01 [24], the shear modulus of the polymer is estimated as: $G = 2.5\,GPa$, and thus the speed of sound in the film is equal to: $c_s \equiv \sqrt{G/\rho} \approx 1580\,m\,s^{-1}$. This yields for the acoustic relaxation time the value of: $\tau_{ac} \approx 63\,ps$. Thus for the $\tau = 10.4\,ps$ laser pulses it is $\tau < \tau_{th}$ and $\tau < \tau_{ac}$ and both conditions for photomechanical ablation are satisfied. It should be mentioned that not all of the thermophysical constants which we had considered above, refer to the exact type of PEDOT:PSS formulation which we use here (CLEVIOS™ FE) but they are characteristics of rather similar types of PEDOT:PSS formulations. The specific heat capacity has the value which we considered above, only at low temperatures and at high temperatures is expected to have a higher value. Nevertheless the above simple calculations provide with a rough estimate of the values of the characteristic times for photomechanical ablation to take place.

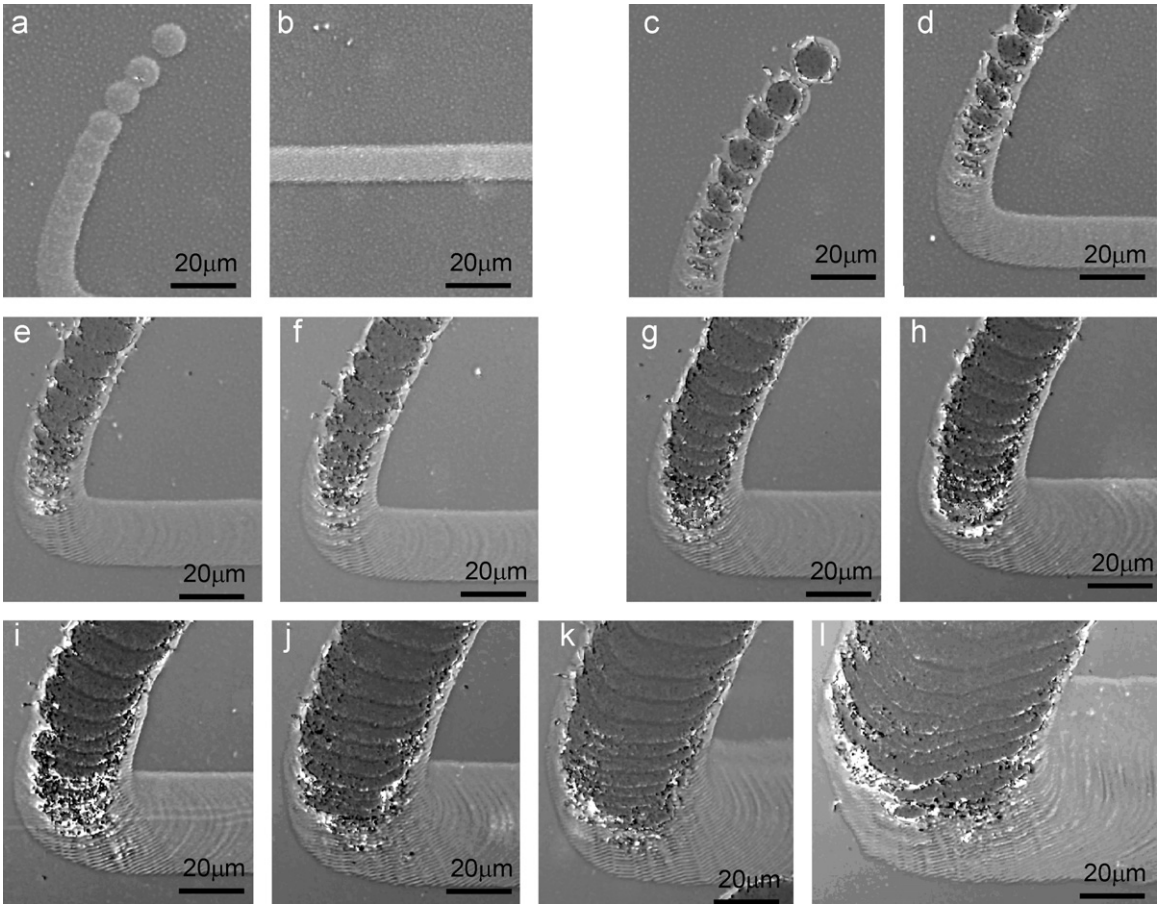

Fig. 4. Typical images of a line patterned on the films (film spin coated at 2000 rpm) at 5 kHz with a low speed of $\upsilon = 5$ mm/s and peak fluences (average power densities) of: 0.15 J/cm² (1.77 W/cm²) (a and b), 0.24 J/cm² (2.84 W/cm²) (c and d), 0.42 J/cm² (4.98 W/cm²) (e), 0.48 J/cm² (5.68 W/cm²) (f), 0.90 J/cm² (10.66 W/cm²) (g), 1.14 J/cm² (13.51 W/cm²) (h), 1.32 J/cm² (15.64 W/cm²) (i), 2.7 J/cm² (32 W/cm²) (j), 4.14 J/cm² (49.06 W/cm²) (k) and 11.01 J/cm² (130.50 W/cm²) (l), respectively.

By applying the well known "square diameter-logarithm fluence" method [25,26], the single pulse ablation thresholds of the films were determined, corresponding to the present picosecond laser ablation. Plots of the measured D^2 versus $\ln(F_0^{pk})$ for the films with different thicknesses are shown in Fig. 2(a). For low fluences (<1.3 J/cm^2) the change of D^2 with $\ln(F_0^{pk})$ for all films follows a straight line in consistency with the "$D^2 - \ln(F_0^{pk})$" method and the ablation thresholds of the films determined from the slopes of those lines are plotted in the graph of Fig. 2(b) versus film thickness. Starting from the thinner films the ablation threshold increases with film thickness almost linearly (a slope of $\sim 1.9 \times 10^{-18}$ J/nm^3), while for films thicker than ~300 nm the ablation threshold exhibits a plateau and does not vary considerably with film thickness.

Following the low fluences region it is seen that for fluences above ~1.3 J/cm^2, the D^2 starts increasing with $\ln(F_0^{pk})$ at a higher rate and does not follow anymore a linear dependence. In this region of fluences the laser energy is so high that the energy penetration depth into the material becomes larger than the optical absorption length. A large portion of the absorbed laser energy by the film, diffuses now as a heat out of the volume where the laser beam was initially incident onto the film surface. This can in turn cause removal of the material, in this high fluences region, with a larger rate versus fluence. For a bulk material with macroscopic dimensions in all three directions, the heat diffuses within the same length in every direction (isotropically) around the irradiated volume, thus the higher material removal rate is inferred only by the higher ablation rate, i.e. the higher rate of increase with the fluence of the depth of ablated craters on the material. However at the present case of thin films (which can be considered as two dimensional systems) with thicknesses comparable to the optical absorption length of the laser radiation in the film material, the heat diffusion length within the film in its vertical direction (perpendicular to the film surface) is limited by the film thickness (the substrate is of a different material than the film) but not in the horizontal directions (parallel to the film surface) where the heat can reach at its maximum diffusion length. Thus the higher material removal rate at the present case of a thin film ablation, reflects to a higher rate of increase with the fluence of rather the diameter of the ablated holes.

For low fluences (<0.15 J/cm^2), no ablation (removal) of the film from the substrate surface is observed but rather blistering (swelling) of the film occurs at the place of incidence of the single laser pulse on the film surface. This indicates that the laser pulse energy is so low that although the portion of the energy which is absorbed by the film and transformed into thermoelastic stress energy is larger than the film adhesion energy (and this results in the peeling-off the film from the substrate), however is not large enough as to cause the build-up of a stress in the film higher than the film minimum fracture strength. In any case, the blisters which are formed onto the film surface under these conditions of low fluences irradiation, provide with an opportunity for an estimation of the minimum PEDOT:PSS film adhesion energy onto a glass substrate. From the measured geometrical characteristics of the formed blisters (height and diameter) and by considering the set of parameters for PEDOT:PSS films: Young's modulus (E_C) = 2.8 ± 0.5 GPa, Poisson ratio (ν_C) = 0.35 ± 0.03, following a sim-

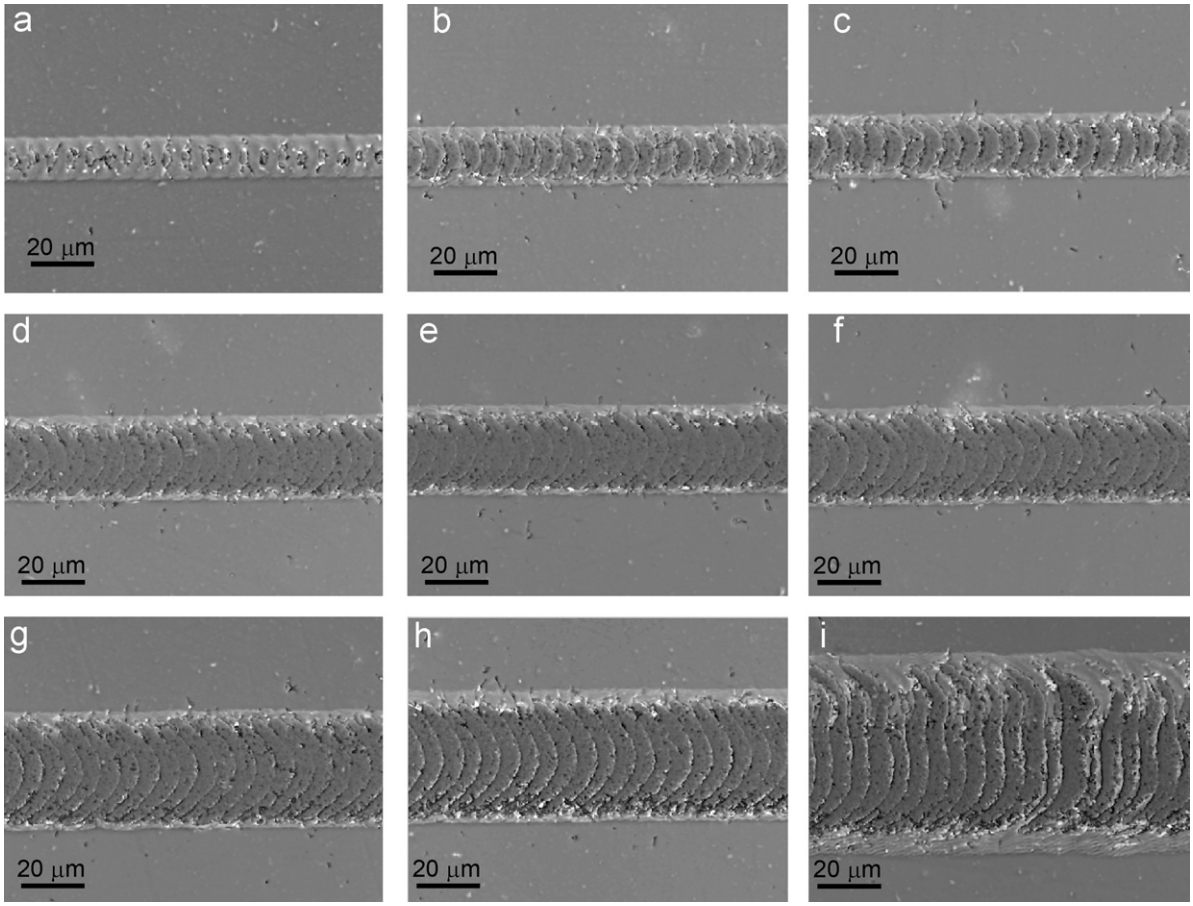

Fig. 5. Typical images of a line patterned on the films (film spin coated at 2000 rpm) at 5 kHz with a speed of υ = 30 mm/s and peak fluences (average power densities) of: 0.24 J/cm^2 (0.47 W/cm^2) (a), 0.42 J/cm^2 (0.83 W/cm^2) (b), 0.48 J/cm^2 (0.95 W/cm^2) (c), 0.90 J/cm^2 (1.78 W/cm^2) (d), 1.14 J/cm^2 (2.26 W/cm^2) (e), 1.32 J/cm^2 (2.61 W/cm^2) (f), 2.70 J/cm^2 (5.35 W/cm^2) (g), 4.14 J/cm^2 (8.20 W/cm^2) (h) and 11.01 J/cm^2 (21.83 W/cm^2) (i), respectively.

ple theory which was developed mainly for blister defects on Ti and TiN coatings on glass [27], the film adhesion energy is estimated equal to $\approx 0.073 \pm 0.005$ μJ/cm^2 (from the data for the film spin coated at 2000 rpm) (image in Fig. 3).

3.2. Patterning of the films by ablation

Picosecond laser ablation patterning of the PEDOT:PSS thin films was carried out by scanning the beam in a line pattern. For low scanning speeds where there is a significant pulse overlap, the film is not ablated even for the highest fluence used but it rather blisters. Ablation of the film is observed only on the areas of incidence of the beam on the film surface where there is no significant pulse overlap, but again for fluences below 0.15 J/cm^2 the film blisters even on the areas where only single pulses are incident on the film surface. This effect is illustrated by the images of Fig. 4 where the beam was scanned with a speed of $\upsilon = 5$ mm/s (at 5 kHz pulse repetition rate) along the straight portions of the lines but at the end of a scanning line it was moved by the mirrors of the SGLV with a progressively higher speed (acceleration of the mirrors) in order to be taken out from the patterning area.

Fig. 5 shows a series of lines patterned using different fluences ($F = 0.24$–2.7 J/cm^2) for the same speed ($\upsilon = 30$ mm/s) at 5 kHz pulse repetition rate. For low fluences (Fig. 5(a) and (b)) the film is photomechanically ablated only at certain points (outside of the regions where there is pulse overlap determined by the scanning speed and fluence) while blistering is observed in the regions where there is a considerable pulse overlap. The removed portions of the film again have the form of flakes rather than a phase changed material (as it was observed in the single pulse ablated holes, Section 3.1). By increasing the fluence further, the total ablated area within the line increases (Fig. 5(c)) but film residues from the ablated areas as well as from the non-ablated areas occupy a large portion of the area within the line. As the fluence increases the film residues accumulate mainly at the sides of the line rather than within the line (Fig. 5(d)). Material accumulates at the edges of the line, in a height of ~210 nm (for $F = 0.9$ J/cm^2, Fig. 5(d)). However for very high fluences large portion of film residues are again obtained within the line (Fig. 5(i)). These residues appear as material which accumulates preferentially around the perimeters of the single pulse traces. It does not have the form of "flakes" anymore but it rather reminds melted and resolidified material possibly due to a large contribution to the polymer film ablation of a phase change mechanism rather than simply photomechanical ablation, at such high peak fluences. These observations indicate that for each scanning speed the peak fluence needs to be increased at a certain value in order to obtain a line with a minimum amount of ablated material residues within its area and as smooth as possible (for instance for $\upsilon = 30$ mm/s this is happening at $F = 0.9$ J/cm^2, Fig. 5(d)). Fig. 2(c) shows the inner and outer width of the line versus peak fluence (bottom scale) and average power density (top scale). The line width increases almost linearly with fluence (with a rate of ~0.03 μm/(J/cm^2)) up to a fluence of ~1.3 J/cm^2 but above that fluence the rate becomes higher, at ~0.26 μm/(J/cm^2). Note that the minimum line width is largely

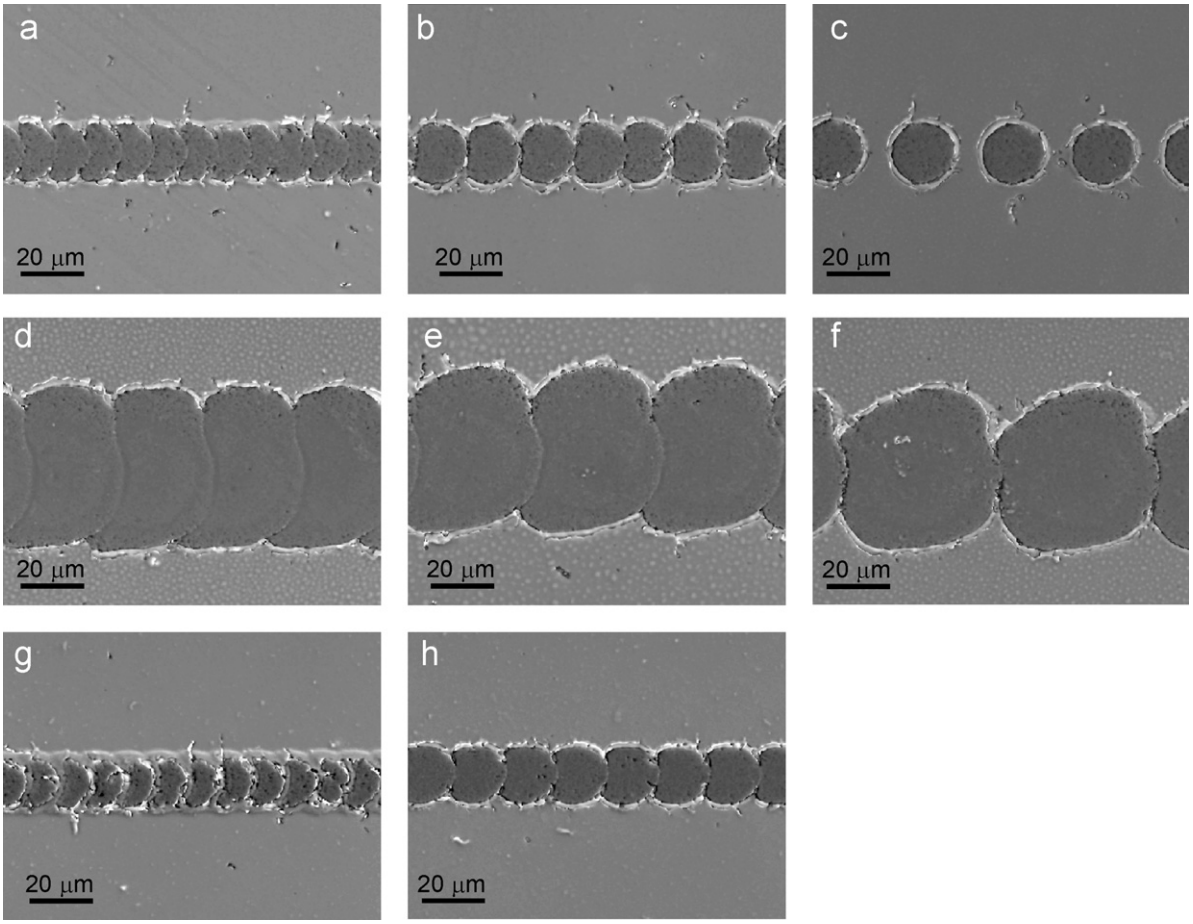

Fig. 6. Typical images of lines patterned on the films (film spin coated at 2000 rpm) at 5 kHz, with a peak fluence of 0.48 J/cm^2 and speeds (average power densities) of: 50 mm/s (0.57 W/cm^2) (a), 80 mm/s (0.35 W/cm^2) (b), and 140 mm/s (0.21 W/cm^2) (c), respectively or with a peak fluence of 6.42 J/cm^2 and speeds (average power densities) of: 140 mm/s (2.73 W/cm^2) (d), 190 mm/s (2.10 W/cm^2) (e), and 240 mm/s (1.60 W/cm^2) (f), respectively or at 50 kHz, with a peak fluence of 0.5 J/cm^2 and speeds (average power densities) of: 500 mm/s (0.62 W/cm^2) (g), and 800 mm/s (0.38 W/cm^2) (h), respectively.

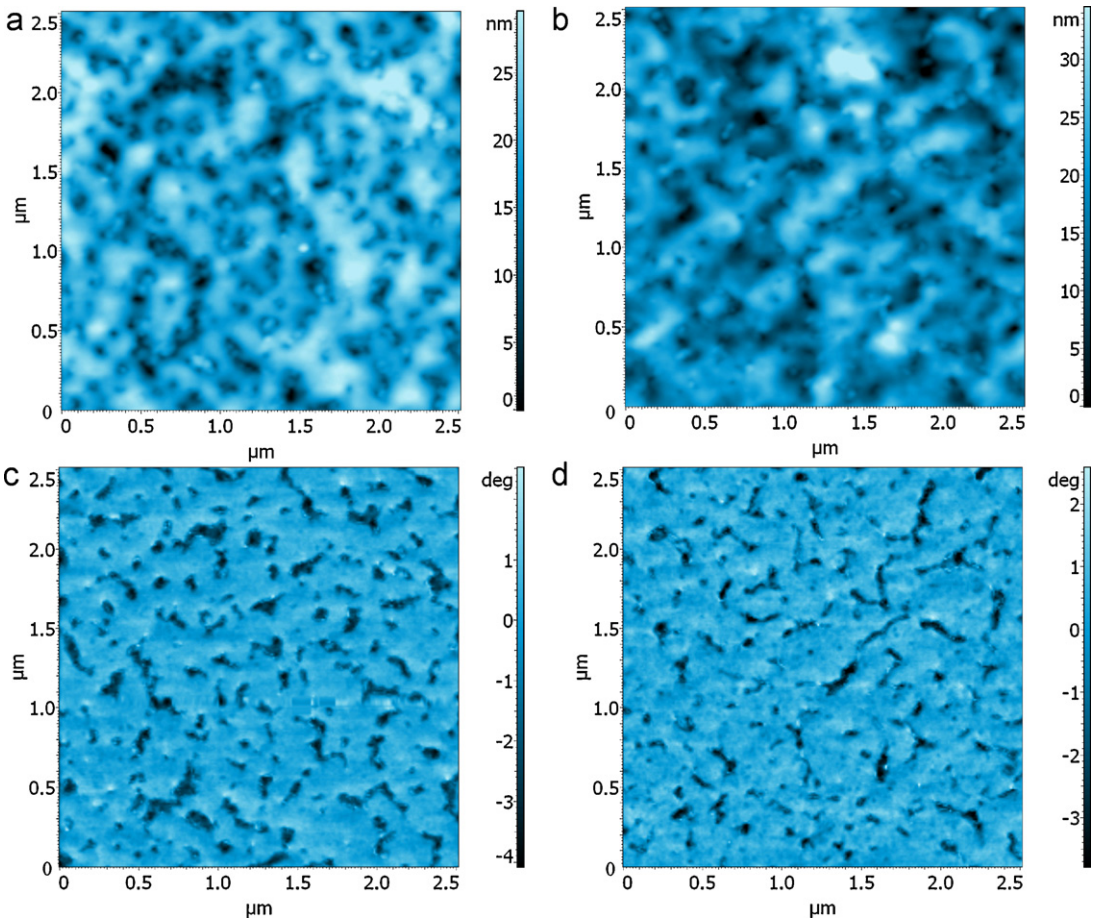

Fig. 7. AFM topography and corresponding phase image of the surface of the unprocessed (a and c) and the irradiated (b and d) films.

determined by the diameter (waist) of the Gaussian laser beam onto the film surface which in turn depends on the focal length of the objective lens which is used to focus the beam. Thus narrower lines are expected to be patterned using a lens with a shorter focal length for beam focusing.

Since for single pulse irradiation in order to obtain removal of the film rather than just blistering, the peak fluence needs to be higher than a certain value, there is an optimum combination of scanning speed and peak fluence in order to have the least joining of single pulse ablated traces which will eventually appear as a continuous, uninterrupted patterned line on the film surface and with a relatively small amount of accumulated material within its inner space area. For instance, when patterning using a fluence of 0.48 J/cm^2 (Figs. 5(c) and 6(a)–(c)) an almost continuous line is still obtained at a maximum speed of 80 mm/s (Fig. 6(b)). For higher fluences (for instance using a fluence of 6.42 J/cm^2, Fig. 6(d)–(f)), continuous lines can be obtained at still higher speeds due to the fact that the diameter of the ablated hole is larger at higher fluences (Fig. 6(f)). However using higher fluences, wider lines are obtained (Fig. 5(c)). Although a continuous line and with an ablation residues-free inner area is also obtained for speeds lower than the optimum one at each fluence (for instance compare Fig. 6(a) with (b)) (as long as the pulse overlap is kept low), the use of higher speeds at each fluence could be preferable from the applications point of view since it leads to a shorter processing time. On the other hand the scalloped profile of the line edges becomes more pronounced at higher speeds but this is not in general considered as an important drawback in for instance applications where laser patterning of the films is carried out just for cutting and separation of two areas of the film (in for example large scale industrial production of optoelectronic devices) [28]. Using higher pulse repetition rates allows the use of even higher speeds in order to obtain the desired results (Fig. 6(g) and (h)). At the same time this also implies a decrease of the processing time by ten times (compare Fig. 6(h) with (b)).

3.3. Laser irradiation of the films before ablation

Laser irradiation of the films (before ablation) was carried out by scanning the beam (at 5 kHz pulse repetition rate) onto the film surface, in a meander fashion, with a speed of $\upsilon = 30$ mm/s, pitch = 1.1 μm, covering a total square area with dimensions of 12×12 mm. The colour of the irradiated film area became light gray as compared to the unprocessed film which was transparent and the appearance of absorption by the film in this range (visible at around ~600 nm) indicates a conversion of the polymer from its oxidized to a reduced form upon laser irradiation [19]. Fig. 7 shows typical AFM images of the surfaces of an unprocessed film and the irradiated one ($F = 0.18$ J/cm^2). The surface of the unprocessed film (Fig. 7(a) and (c)) exhibits the characteristic surface morphology of PEDOT:PSS films consisting of grains (PEDOT-rich regions) and large areas among them which appear almost featureless (PSS-rich regions) [29,30]. The surface morphology of the irradiated film (Fig. 7(b) and (d)) also appears not much different. This indicates that the surface morphology of the film does not change considerably upon laser irradiation under the present conditions of irradiation.

The resistance of the unprocessed film was measured equal to $478 \pm 80.9\ \Omega$ (conductivity = 163 ± 28 S/cm), however the resistance of the laser irradiated film was infinite and thus the film was

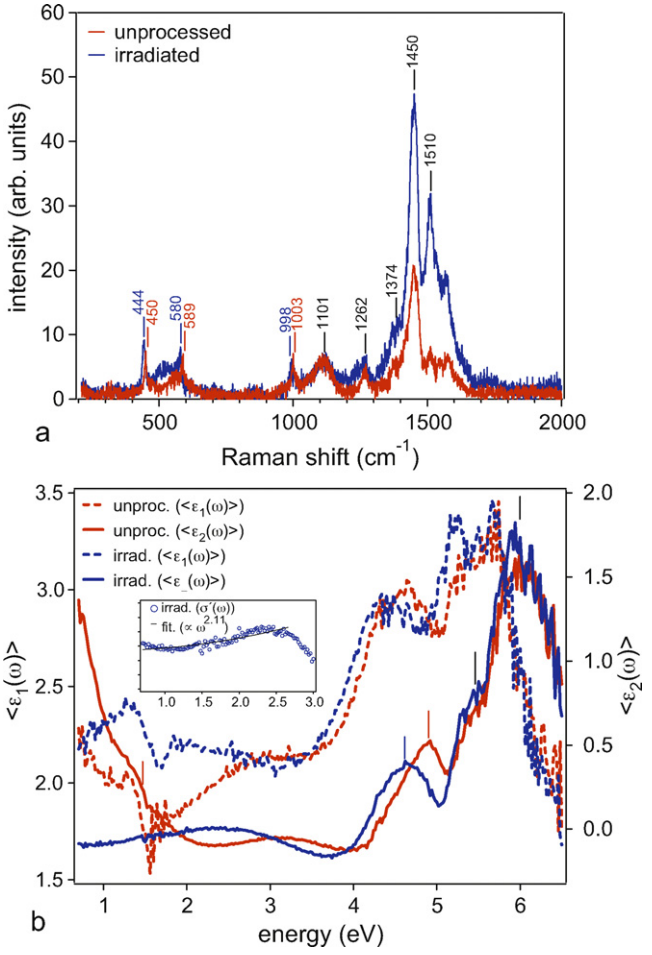

Fig. 8. Raman (a) and Spectroscopic Ellipsometry (b) spectra measured from the unprocessed and laser irradiated films. Inset in (b) shows the calculated optical conductivity in the low energies region.

exhibiting an insulating behaviour. To obtain information about the possible reasons for the increase of the resistance of the irradiated film to infinity, we have carried out Raman spectroscopy and Spectroscopic Ellipsometry on the films. Raman spectra of the unprocessed and the laser irradiated film in the whole spectral region 200–2000 cm^{-1} are shown in Fig. 8(a). The observed peaks in the spectra are identified in Table 1 based on reports in the literature [31,32]. Analysis of the spectra, first in the region 1300–1600 cm^{-1} where the C_α=C_β stretching vibrational modes appears, shows that the ratio of the intensities of the band corresponding to the symmetric C_α=C_β mode at 1510 cm^{-1} and of the band corresponding to the asymmetric one at 1450 cm^{-1}, is larger for the irradiated film ($(I_{symm}/I_{assym})^{irrad} = 2.93$) than for the unprocessed one ($(I_{symm}/I_{assym})^{unproc} = 1.54$). Although for PEDOT:PSS thin films a direct correlation between the intensities ratio of the two bands and the conductivity does not yet exist in the literature, however an increase of the ratio of the intensities of the two bands which we observe here for the irradiated film might explain the significant decrease of the conductivity consistent with a decrease of the polymer conjugation length in agreement with similar observations made for thiophene films [33] or PEDOT nanofibers [34]. A further observation of the spectra in the region 400–1100 cm^{-1} shows that the band corresponding to the SO_2 bending mode as well as the ones corresponding to the oxyethylene ring deformation which in the spectrum of the unprocessed film appear at 450, 589 and 1003 cm^{-1} respectively, in the spectrum of the irradiated film appear at lower wavenumbers, at 444, 558, and 998 cm^{-1}, respectively. These shifts again might be consistent with a possible shortening of the conjugation length of the neutral parts of the polymer [35] or even a polymer chain scission.

Table 1
Vibrational modes in the Raman spectra of the unprocessed and laser irradiated PEDOT:PSS films.

Vibr. mode freq. (cm^{-1})		Assignment
Unprocessed	Irradiated	
1510	1510	Asymmetric C_α=C_β stretching
1450	1450	Symmetric C_α=C_β (–O) stretching
1374	1374	C_β–C_β stretching
1262	1262	C_α–$C_{\alpha'}$ (inter-ring) stretching
1101	1101	C–O–C deformation
1003	998	Oxyethylene ring deformation
589	580	Oxyethylene ring deformation
450	444	SO_2 bending

The real and imaginary parts of the pseudodielectric function: $\langle\varepsilon(\omega)\rangle \equiv \langle\varepsilon_1(\omega)\rangle + i\langle\varepsilon_2(\omega)\rangle$ of the unprocessed and the laser irradiated film, measured by SE, are shown in Fig. 8(b). The bands at ~5.46 and ~5.98 eV are due to π–π* intraband electronic transition in the benzene ring of the PSS and they appear at almost the same energy in the spectra of the two films. The broad band which in the spectrum of the unprocessed film appears to be centered at ~4.92 eV is due to an overlap of the transition from the ground state (S0) to the first excited state (S1) for PEDOT (which is supposed to appear at 4.98 eV) and of the excitation of the PSS molecule from its ground state (S0) to the first excited state (S1) due to the transfer of electron from HOMO to LUMO (which is supposed to appear at 4.85 eV). The oscillator strength of the PEDOT transition is greater than the oscillator strength of the PSS transition and therefore this band can be considered to be due almost completely to the PEDOT transition [36]. This band appears to be shifted to lower energies (and centered at ~4.62 eV) in the spectrum of the irradiated film. Furthermore and most importantly a dramatic difference between the spectra of the two films is observed in the low energies region, below ~3 eV. In the spectrum of the unprocessed film there is a constantly increasing absorption in the region below ~1 eV as well as a broad band centered at ~1.5 eV. These features denote a state of the polymer with a high conductivity and are characteristics of metallic polymers, in general. In the metallic state of the polymer the Fermi level is at the centre of the highest occupied (conduction) band and there are two well defined contributions to the spectra; intraband excitations due to the free carrier plasma resonance because of the presence of bipolarons which appear as contributions to the lowest energies part of the spectra below ~1 eV and interband contributions from the Fermi level to the next higher empty band (or to a transition from a lower lying filled band to the Fermi level) which appear as a band centered at ~1.5 eV [37,36]. However, in the spectrum of the irradiated film these low energy features are not present and $\langle\varepsilon_2(\omega)\rangle$ exhibits a slow decrease with decreasing energy. This is a prominent feature of a polymer which is in the state of a so-called Fermi glass and exhibits an insulating behaviour because of the localization of all electronic states at the Fermi level due to the charge carriers localization. By considering furthermore the real part of the optical conductivity $\sigma'(\omega)$ which is related to $\varepsilon_2(\omega)$ through the relation: $\sigma'(\omega) \propto \omega\varepsilon_2(\omega)$, it is readily seen that in the low energies region, $\sigma'(\omega)$ follows a dependence on ω of the form of ω^s with $s = 2.11$ (inset in Fig. 8(b)) which is very close to the ω^2 (i.e. with $s = 2$) dependence which is expected for a Fermi glass according to the localization theory [38,39]. This change of the polymer film from the metallic to an insulating regime indicates a polymer metal–insulator transition (MIT) induced by the laser radiation in analogy to a similar transition induced by a heat-annealing process of the PEDOT:PSS films [40]. It might be possible that laser irradiation of the polymer destroys the planar geometry

of the thiophene and oxyethylene rings (thus the shift to different energies of the bands corresponding to the oxyethelene ring and of the SO_2 bending vibrations which is seen in the Raman spectra (Fig. 8(a))), which in turn causes a molecular scale disorder and a reduction of the polymer conjugation length. At the same time laser irradiation also induces a splitting of the bipolarons and formation of polarons. This molecular disorder has as a result the charge carrier localization in the PEDOT and thus the localization of electronic states near the Fermi level.

4. Conclusions

In conclusion, photomechanical ablation is the likely ablation mechanism of PEDOT:PSS thin films (spin coated on glass substrates) using a 10.4 ps (1064 nm) laser source. The single pulse ablation thresholds were measured equal to 0.13–0.18 J/cm^2 for films with thicknesses in the region of ~100–600 nm. Films with thickness greater than ~300 nm are behaving as bulk materials in terms of the current picosecond laser ablation (at low fluences). When line pattering using low fluences and low scanning speeds (where there is a considerable pulse overlap), blistering of the film is observed, instead of removal. Laser irradiation of the films (before ablation) causes a metal–insulator transition of the polymer possibly due to the creation of molecular disorder which in turn results in charge localization.

Acknowledgements

This work was performed within the framework of a Marie Curie Fellowship of the European Community, Grant number MTKD-CT-2004-517165 and a European Reintegration Grant (ERG) number PERG03-GA-2008-226029, 83573 and it was carried out with the assistance of the North West Laser Engineering Consortium (www.nwlec.org.uk) a project funded by the North West Development Agency (NWDA) in the UK.

References

[1] S. Kirchmeyer, K. Reuter, J. Mater. Chem. 15 (2005) 2077.
[2] S.-I. Na, S.-S. Kim, D.-Y. Kim, Adv. Mater. 20 (2008) 4061.
[3] M. Okano, K. Itoh, A. Fujishima, J. Electrochem. Soc. 134 (1987) 837.
[4] P. Tehrani, N.D. Robinson, T. Kugler, T. Remonen, L.-O. Hennerdal, J. Hall, A. Malmstrom, L. Leenders, M. Berggren, Smart Mater. Struct. 14 (2005) 21.
[5] D. Hohnholz, H. Okuzaki, A.G. MacDiarmid, Adv. Funct. Mater. 15 (2005) 51.
[6] A. Colsmann, F. Stenzel, G. Balthasar, H. Do, U. Lemmer, Thin Solid Films 517 (2009) 1750.
[7] H. Kumagai, K. Midorikawa, K. Toyoda, S. Nakamura, T. Okamoto, M. Obara, Appl. Phys. Lett. 65 (1994) 1850.
[8] S. Küper, M. Stuke, Appl. Phys. Lett. 54 (1989) 4.
[9] J. Heitz, E. Arenholz, D. Bäuerle, R. Sauerbrey, H.M. Phillips, Appl. Phys. A 59 (1994) 289.
[10] S. Baudach, J. Bonse, W. Kautek, Appl. Phys. A 69 (1999) S395.
[11] D.E. Hare, J. Franken, D.D. Dlott, J. Appl. Phys. 77 (1995) 5950.
[12] P. Lemoine, J.D. Magan, W. Blau, Microelectr. Eng. 13 (1991) 447.
[13] J.P. MacDonald, J.L. Hendricks, V.R. Mistry, D.C. Martin, S.M. Yalisove, J. Appl. Phys. 102 (2007) 013107.
[14] T. Feurer, R. Sauerbrey, M.C. Smayling, B.J. Story, Appl. Phys. A 56 (1993) 275.
[15] R. Baumann, J. Bargon, Appl. Surf. Sci. 106 (1996) 287.
[16] C. Wochnowski, S. Metev, G. Sepold, Appl. Surf. Sci. 154 (2000) 706.
[17] J. Kleinbauer, R. Knappe, R. Wallenstein, Appl. Phys. B 80 (2005) 315.
[18] http://www.hcstarck.com/.
[19] G. Sonmez, Chem. Commun. (2005) 5251.
[20] L.J. Van der Pauw, Philips Res. Rep. 13 (1958) 1.
[21] G. Paltauf, P.E. Dyer, Chem. Rev. 103 (2003) 487.
[22] J.F. Xing, X.J. Kun, L.B. Yang, X. Yu, H.R. Jin, L.L. Feng, Chin. Phys. Lett. 25 (2008) 2202.
[23] P.K. Kahol, J.C. Ho, Y.Y. Chen, C.R. Wang, S. Neeleshwar, C.B. Tsai, B. Wessling, Synth. Met. 153 (2005) 169.
[24] U. Lang, N. Naujoks, J. Dual, Synth. Met. 159 (2009) 473.
[25] J. Bonse, J.M. Wrobel, J. Krüger, W. Kautek, Appl. Phys. A 72 (2001) 89.
[26] J.M. Liu, Opt. Lett. 7 (1982) 196.
[27] S.G. Koulikov, D.D. Dlott, J. Photochem. Photoobiol. A: Chem. 145 (2001) 183.
[28] Lasers in Photovoltaics Manufacturing, Industrial Laser Solutions, vol. 24, issue 12, December 2009.
[29] X. Crispin, F.L.E. Jakobsson, A. Crispin, P.C.M. Grim, P. Anderson, A. Volodin, C. van Haesendonck, M. Van der Auweraer, W.R. Salaneck, M. Berggren, Chem. Mater. 18 (2006) 4354.
[30] Y.-S. Hsiao, W.-T. Whang, C.-P. Chen, Y.-C. Chen, J. Mater. Chem. 18 (2008) 5948.
[31] W.W. Chiu, J. Travaš-Sejdić, R.P. Cooney, G.A. Bowmaker, J. Raman Spectrosc. 37 (2006) 1354.
[32] S. Garreau, G. Louarn, J.P. Buisson, G. Froyer, S. Lefrant, Macromolecules 32 (1999) 6807.
[33] M. Akimoto, Y. Furukawa, H. Takeuchi, I. Harada, Y. Soma, M. Soma, Synth. Met. 15 (1986) 353.
[34] J.L. Duvail, P. Rétho, S. Garreau, G. Louarn, C. Godon, S. Demoustier-Champagne, Synth. Met. 131 (2002) 123.
[35] S. Sakamoto, M. Okumura, Z. Zhao, Y. Fukurawa, Chem. Phys. Lett. 412 (2005) 395.
[36] G. Agalya, C. Lv, X. Wang, M. Koyoma, M. Kubo, A. Miyamoto, Appl. Surf. Sci. 244 (2005) 195.
[37] Y. Chang, K. Lee, R. Kiebooms, A. Aleshin, A.J. Heeger, Synth. Met. 105 (1999) 203.
[38] N.F. Mott, Metal–Insulator Transitions, Taylor and Francis, New York, 1990.
[39] K. Lee, A.J. Heeger, Y. Cao, Synth. Met. 72 (1995) 25.
[40] S. Cho, S.H. Park, K. Lee, J. Kor. Phys. Soc. 47 (2005) 474.